# Electronic-structure calculations for the $Mo_3(D_{3h})$ unit and its successive finite condensations $Mo_6(D_{3h},D_{3d},O_h)$, $Mo_9(D_{3h})$, and $Mo_{12}(D_{3d})$ up to the infinite chain $(Mo_{6/2})^1_\infty$

A. Le Beuze, P. Lamandé, and R. Lissillour
*Laboratoire de Chimie Théorique,* Université de Rennes I—Campus de Beaulieu, 35042-Rennes Cédex, France*

H. Chermette
*Institut de Physique Nucléaire (et Institut National de Physique Nucléaire et de Physique des Particules, IN2P3), Université de Lyon I, 43 Boulevard du 11 Novembre 1918, 69622-Villeurbanne Cédex, France*

(Received 28 November 1983; revised manuscript received 30 July 1984)

Self-consistent-field $X\alpha$ scattered-wave molecular-orbital calculations have been performed for molybdenum clusters containing one, two, three, and four trimetallic triangles in a stacked configuration. The bonding interactions of the parent $Mo_3$ layer are discussed in detail and the corresponding energy diagram is analyzed as arising mainly from the superposition of two sets of Walsh-like orbitals. In the $Mo_6$ clusters the interlayer interactions arising from the staggered ($D_{3d}$) stacking mode, as well as the eclipsed ($D_{3h}$) alternative, are analyzed. With increasing cluster size, up to $Mo_9$ and $Mo_{12}$, emphasis is placed on a convergence behavior in the electronic patterns. Moreover, we could observe localized $d$-electron states which appear to be analogous to the surface states of the crystals. Finally, an energy-band scheme, derived from finite-cluster molecular orbitals, is presented in the case of a linear chain, arising from an infinite condensation of $Mo_3$ layers. A high density of states occurs at the Fermi level. Moreover, it is crossed by a broad half-filled $a_2$ band ($xz$ orbitals), giving rise to quasi-one-dimensional conductor character. These electronic factors generate an instability situation, the well-known Peierls distortion, characteristic of such pseudolinear chains. An analysis of this structural unstability is given by calculations performed on distorted $Mo_{12}$ units constructed by the juxtaposition of two $Mo_6$ fragments. This last study allows us (i) to elucidate the important change in the electronic structure with the occurrence of a large energy gap just above the Fermi level, and (ii) to present an alternative route to the energy-band scheme of the infinite chain.

## I. INTRODUCTION

Compounds containing discrete metal clusters (i.e., molecular clusters) are the focus of increasing activity in inorganic chemistry as well as in solid-state chemistry.[1,2] Thus molybdenum chemistry has become today a rich field of extended metal-metal bonding systems.[3,4] Those molybdenum clusters provide a unique logical connection between the realms of coordination and solid-state chemistry with that of small aggregates of atoms.[5] Furthermore, it has been referred to as cluster science.[6]

In any case, the electronic structure of those materials are expected to be influenced by metal-metal interactions. So it seems basic to the understanding of the condensed state of the compounds to know how electronic and other properties change when metal atoms come together to build up the clusters.

In this paper we are interested in molybdenum systems whose molecular frame may be considered a one-dimensional (1D) condensation of discrete triangular $Mo_3$ layers giving rise to a stacked cluster.[4,7] These species provide a particularly attractive opportunity to study the successive condensation of $Mo_3$ layers, up to the formation of an extended linear chain.

For this purpose we have carried out self-consistent-field $X\alpha$ scattered-wave (SW) calculations. Section II of this paper deals with the models and the SCF $X\alpha$ SW method. In the following sections, we present results for the bare molybdenum clusters $Mo_3(D_{3h})$, $Mo_6(D_{3h},D_{3d},O_h)$, $Mo_9(D_{3h})$, and $Mo_{12}(D_{3d})$, as well as a band-structure scheme, derived from our cluster calculations, concerning a pseudolinear metallic chain $(Mo_3)^1_\infty$. Finally, the instability of the regular chain against dimerization is analyzed.

## II. MODELS AND COMPUTATIONAL DETAILS

In all the compounds reported, the molybdenum atoms form equilateral triangles with a Mo—Mo distance of about 2.7 Å. In our study we used the structural data observed in Potel's linear-chain compound $Tl_2Mo_6Se_6$ (Ref. 4) (i.e., $d_{Mo\text{-}Mo}$ intralayer equals 2.663 Å, $d_{Mo\text{-}Mo}$ interlayer equals 2.725 Å, $d$ interlayer equals 2.250 Å). The clusters were placed in a coordinate system with the $z$ axis perpendicular to the metal triangles (see Fig. 1).

The molecular-orbital calculations were performed by means of the SCF SW $X\alpha$ approach. This method is based on the local exchange-correlation functional, through Slater's $X\alpha$ approximation, and on the multiple-scattered-wave method for solving the one-electron Schrödinger equations. This procedure is well documented,[8] and we have recently shown that it provides a convenient approach for describing the electronic structure of this type of cluster.[9]

 

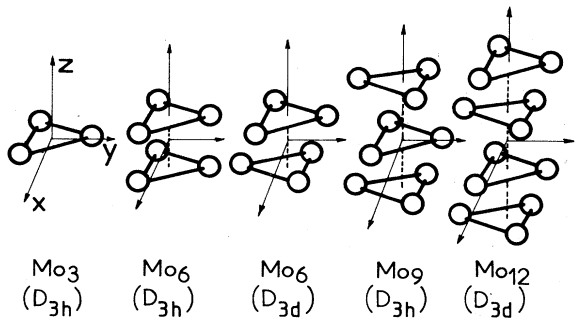


FIG. 1. Models used for the calculations.

The $\alpha$ values for Mo ($\alpha=0.703\,41$) were obtained from the Schwarz tabulation.[10] The same $\alpha$ value was used for inter- and outer-sphere regions. The initial molecular potential was a superposition of Herman-Skillman atomic potentials.[11] The molybdenum spheres radii ($R_{\mathrm{Mo}}=2.8840$ a.u.) were chosen in order to allow an overlap of about 12% along the Mo—Mo distances in the triangles. The outer-sphere radii were taken to be tangential to the outermost atomic spheres. The SCF calculations were made to converge to less than $\pm 0.001$ Ry on each level, and the core levels were relaxed as proposed by Gubanov[12] (i.e., their atomic character was kept, but their energies and density distributions were allowed to vary through the self-consistent procedure). The symmetry-adapted linear combinations of atomic orbitals included $s,p,d$ spherical harmonics on Mo, and spherical harmonics up to $l=4$ on the outer sphere. No relativistic corrections were included throughout the calculations, since the effect on the Mo valence orbital is quite small[9] and therefore the trends in the chemical bonding can be obtained with a smaller computational effort.

## III. RESULTS AND DISCUSSION

### A. $Mo_3$ cluster

There has been much effort expended trying to provide detailed electronic descriptions of the bonding in trimetallic systems, as well as for bare metal clusters[1,13] and trinuclear metal complexes.[14] However, little work[15] has been done on molybdenum units. So, it would appear useful for us to gain a clear understanding of the bonding mechanism in the $Mo_3$ unit, especially as we will take it as the parent fragment to build up the larger clusters.

Energies and charge distributions, restricted to the valence levels, are presented in Fig. 2. Contour maps of some molecular orbitals (MO's) are drawn in Fig. 3. In fact, the levels can be gathered into six low-lying bonding or nonbonding states and five high-lying antibonding states.

The $z$ axis being perpendicular to the triangular plane, one can therefore formally separate the levels between $\sigma$'s—showing bonding or antibonding in-plane $(x,y)$ interactions—from $\pi$'s—having out-of-plane $(z)$ components. In this way, the energetically lower $1a_1'$ MO's present $d\sigma$ interactions with a large contribution from

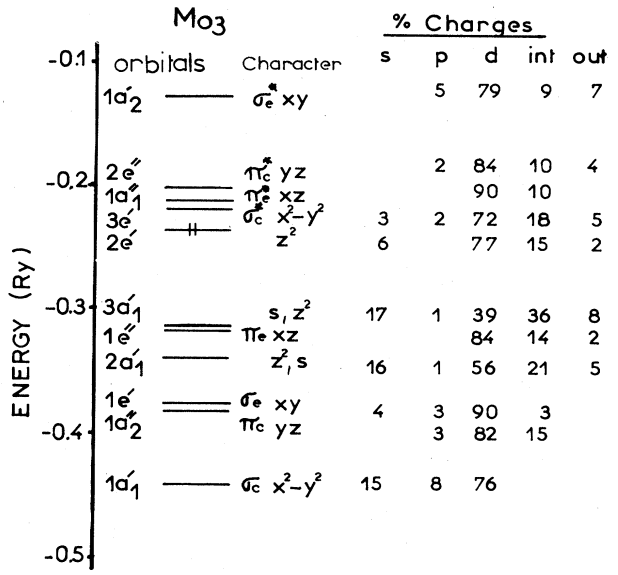


FIG. 2. Energy and charge (%) of the valence levels of $Mo_3$.

$d_{x^2-y^2}$ orbitals. This results in a strong three-center $\sigma$-bonding orbital directed towards the cluster center ($\sigma_c$). The $1e'$ MO with $d_{xy}$ character is the second $\sigma$-type bonding level but corresponds to bonds directed along the edges of the triangle ($\sigma_e$).

The low-lying $\pi$-type bonding level is the $1a_2''$ MO with $d_{yz}$ atomic-orbital components; it equally shows a three-center delocalization ($\pi_c$). The combination of metal $d_{xz}$ orbitals is expected to result in a small metal-metal overlap, which explains the weak bonding character of the $1e''$ MO ($\pi_e$). Finally, $d_{z^2}$ atomic orbitals concern mainly the $3a_1'$ and $2e'$ MO's which are, respectively, nonbonding and antibonding.

We notice that some of the filled levels contain a significant amount of $5s$ character arising from the hybridization of $4d$ states which belong to the same irreducible representations $a_1'$ and $e'$. Thus the $3a_1'$ MO which displays the higher $s$ population in the atomic sphere, with respect to the $d$ one, must be associated with the $a_1'$ MO $5s$ state. So the Mo $5s$ atomic orbitals, as well as the Mo $5p$ ones, play a substantial role in the bonding of the $Mo_3$ unit.

Figure 3 permits us to clarify our understanding of all those interactions and to have a picture of the chemical bonding. Indeed, the contour maps provide a meaningful description of the overall metal-metal interactions, which let us consider the MO diagram pattern as mainly arising from superposition of two sets of Walsh-like $d$ orbitals[16] analogous to the Walsh orbitals of cyclopropane.[17] Indeed, the first set is a $\sigma$-$\sigma^*$ one, with $(1a_1'+3e')$ and $(1e'+1a_2')$ orbitals, respectively, while the second is a $\pi$-$\pi^*$ type with $(1a_2''+2e'')$ and $(1e''+1a_1'')$ orbitals (see Fig. 3).

Each of these bonding sets $(\sigma,\pi)$ of Walsh-like orbitals is filled with six electrons. The bonding between each couple of Mo atoms corresponds then to a $1\sigma+1\pi$ bond plus a weaker bonding contribution from the two elec-

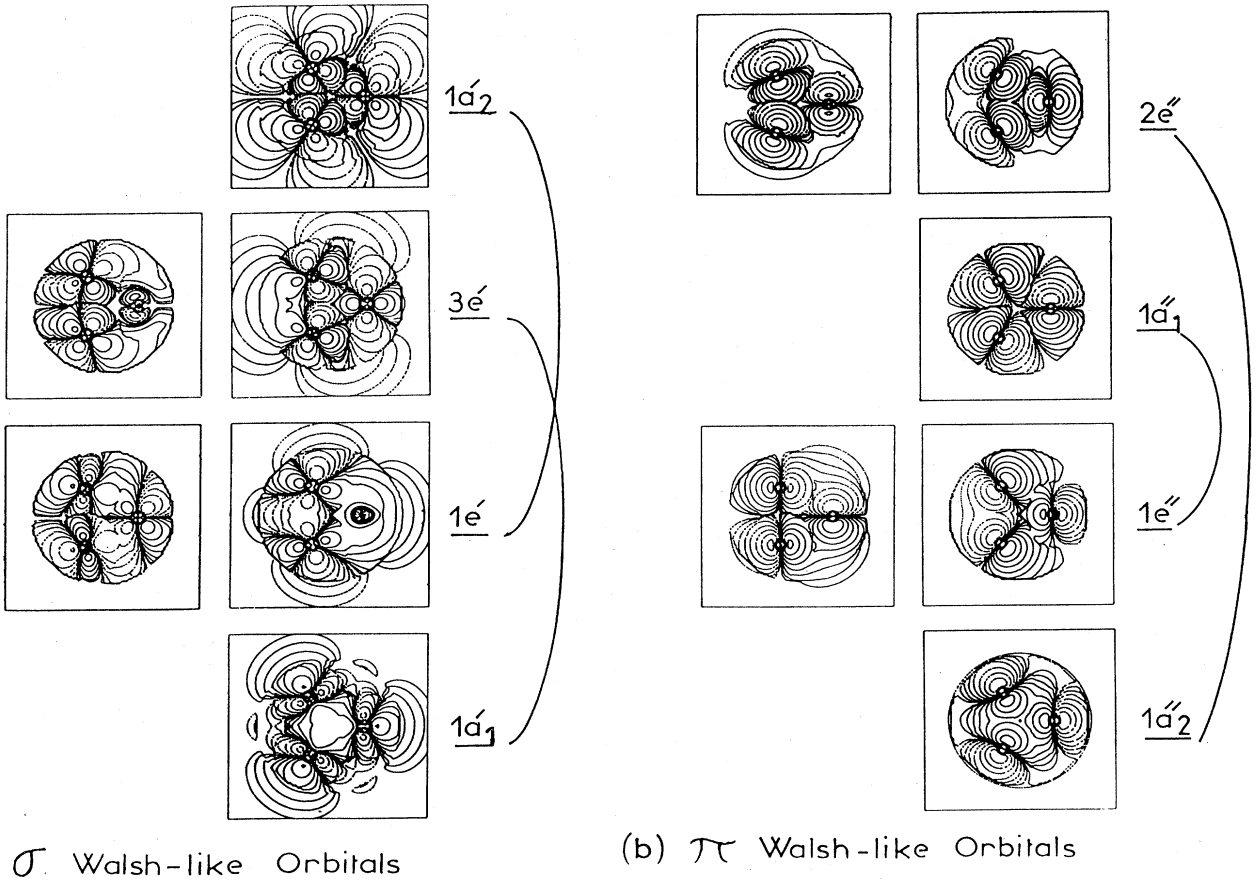


FIG. 3. (a) $\sigma$ Walsh-like orbitals (see test for comments). The continuous contour line corresponds to a positive wave function and the dotted contour line to a negative one. (b) $\pi$ Walsh-like orbitals. The curve corresponds to a plane situated at 0.1 a.u. above the trimetallic nodal plane.

trons of the $3a_1'$ MO with $5s$ character. Indeed, the half-occupation of the $2e'(d_{z^2})$ MO counterweights the two electrons of the $2a_1'$ MO.

### B. $Mo_6$ ($D_{3h}$,$D_{3d}$,$O_h$) clusters

We now describe how two triangular metal rings can stack together and why $D_{3d}$ clustering (i.e., staggered rings rotated by 60°) is energetically favored with respect to the $D_{3h}$ alternative (i.e., the rings fit perfectly), all other things being equal (e.g., interlayer separation, metal distance within the layer, total number of electrons).

Stacking together two $Mo_3$ triangles results—in a first approximation—in the interaction of each MO of one ring with the equivalent MO of the second ring. Indeed, the nearer the energy of the interacting MO's, the stronger the interaction.

First, the energy diagram depicted in Fig. 4 illustrates that, whatever the stacking mode, all these combinations are obedient to the symmetry rules. An in-phase combination, denoted as $(++)$, of $\sigma$-$Mo_3$ levels, which are symmetric with respect to the metal plane, leads to symmetric $Mo_6$ MO denoted by $(S)$ (i.e., with respect to the median plane $xy$ for $D_{3h}$ and to the reversing point for $D_{3d}$), while out-of-phase combination $(+-)$ gives rise to antisymmetric $Mo_6$ MO $(A)$. The inverted combination must then occur for $\pi$-$Mo_3$ MO's:

$$\sigma \text{ levels: } (++)\rightarrow(S),\ (+-)\rightarrow(A)\ ,$$

$$\pi \text{ levels: } (++)\rightarrow(A),\ (+-)\rightarrow(S)\ .$$

The combination of $\pi$-$Mo_3$ orbitals is expected to produce a larger overlap than $\sigma$ ones which are more localized in the layer plane. So, whatever the stacking mode ($D_{3h}$ or $D_{3d}$) may be, building a $Mo_6$ cluster with the $Mo_3$ parent should be largely governed by interactions between $\pi$-layer orbitals. Indeed, the better the MO's overlap, the stronger the interaction. This is clearly reflected in Fig. 4 where levels arising from one $\pi$-$Mo_3$ MO are more energetically divided than those parented to a $\sigma$-$Mo_3$ one. In Fig. 5 we have drawn contour maps of the low-lying $\pi$-type ($d_{yz}$) $1a_{1g}$ ($D_{3d}$) and $1a_1'$ ($D_{3h}$) MO's. Both, mainly parented to the $\pi$-$1a_2''$ $Mo_3$, contribute largely to significant metal-metal bonding of the $Mo_6$ units with an almost equal strength. Indeed, the motion relating the staggered to the eclipsed forms leaves the threefold axis intact. This means that $\pi$-$Mo_3$—centered orbitals (i.e., mainly localized

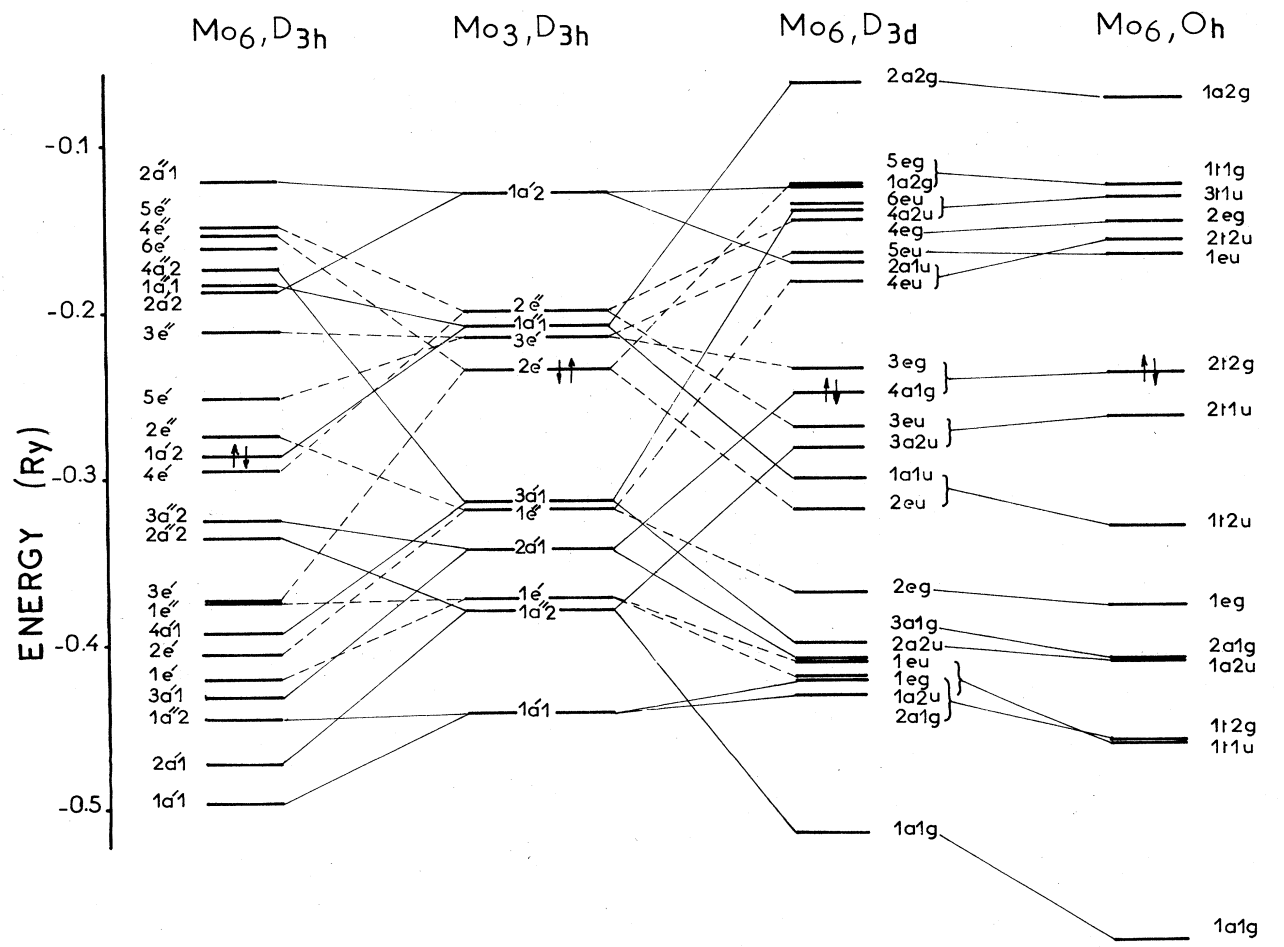


FIG. 4. Ground-state energy levels of the $Mo_6$ clusters. Arrows indicate the population of the highest filled level.

on the central axis) give rise to interlayer interactions which are little, if at all, sensitive to the configuration. However, we can note a better cluster-centered character of the $1a_{1g}$ orbital favoring the $D_{3d}$ form. This is further evidenced by the lower energy of this MO.

Unlike those $d_{yz}$ orbitals, the ones localized along the edges, or at the vertex, of $Mo_3$ triangles lead to the main differences between the two cluster forms. Indeed, if the symmetry-adapted combinations lead again to analogous symmetry-type MO's, the nature (bonding or antibonding) and the strength of the interlayer interactions change nevertheless. For instance, we discuss first the bonding interactions arising from $d_{z^2}$ orbitals. Thus, unlike the $D_{3h}$ condensation, the $D_{3d}$ symmetric level $4a_{1g}$ becomes interlayer antibonding ($SA$) in the aggregates. As outlined in Fig. 6, the $d_{z^2}$ lobes of one $Mo_3$ plane directly interact with the inverted-sign component of the wave function localized in the edge of the other $Mo_3$ triangle.

Another pertinent example is in the important inverted character of the bonding interactions resulting from the combination of $d_{xz}$ orbitals (e.g., $\pi_e^*$-$1a_1''$ $Mo_3$ MO). The bond strength plays an important role as a driving force favoring the staggered condensation. As depicted in Fig. 7 the $\pi$ interplanar bonding mode leads to a $\pi$ metal-metal bond for $D_{3h}$ ($1a_2'$) which does not match the strong $\sigma$ metal-metal bond obtained for $D_{3d}$ ($1a_{1u}$). This is a consequence of the larger overlap between $d_{xz}$ orbitals of the staggered triangles.

All this symmetry-based analysis remains, however, largely unrefined because it does not point out the actual strong rehybridization of the $Mo_3$ orbitals when two triangle units stack together. Indeed a large symmetry-allowed $\sigma$-$\pi$ mixing occurs among $Mo_3$ wave functions. This is illustrated, for instance, in Fig. 5 where the $Mo_6$ cluster orbitals should be imagined as hybrid combinations arising from several parents which are mainly $\pi_c$ and $\sigma_c$ in character, as well as from $5s$ and $5p$ orbitals. It is evident that this mixing takes place in order to homogenize the intra- and interlayer interactions.

Although the $X\alpha$ SW method displays only limited accuracy for the total energies, the relative values for such closely related clusters should be meaningful. The binding energy per Mo atom is reported in Table I. The results obtained show several interesting trends. There is, at first, an increase in the binding energy per Mo atom as the size of the cluster increases and as the symmetry changes from $D_{3h}$ to $D_{3d}$. On the other hand, in spite of the diminution of the bond energy by passing from $D_{3h}$ to $D_{3d}$, the energetic observations favor the $D_{3d}$ configuration (see columns 3 and 5 of Table I). This is clearly reflected by

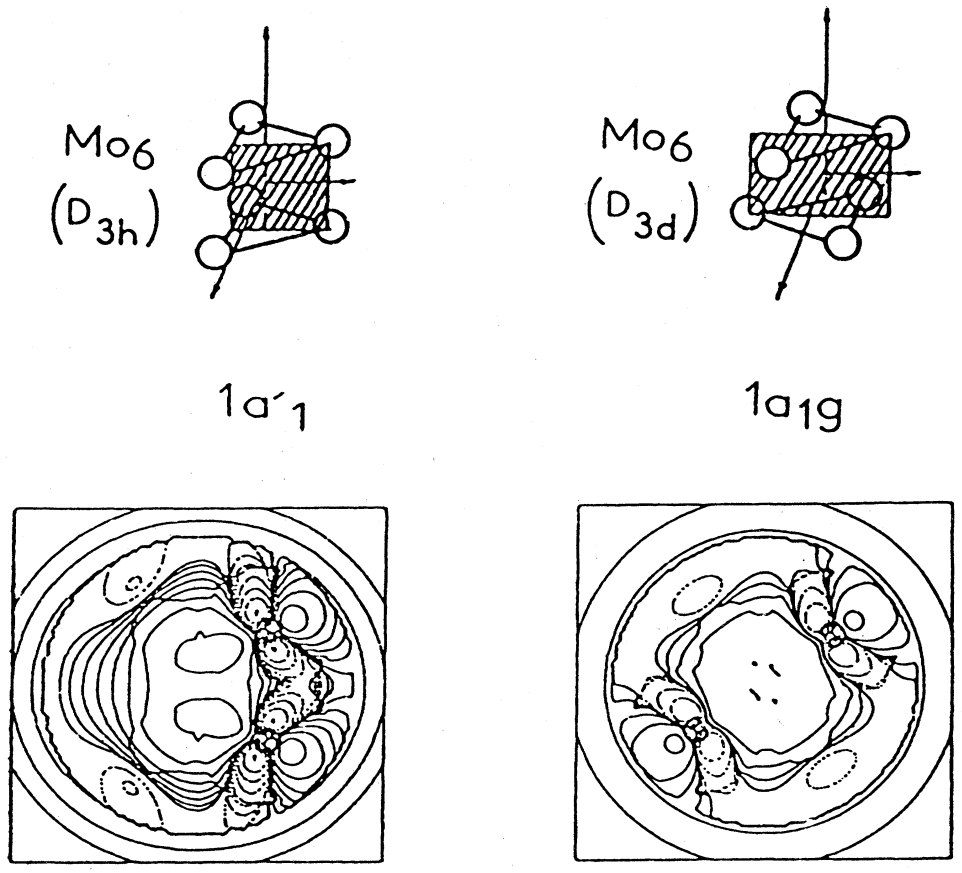


FIG. 5. Wave-function contours of low-lying levels of $Mo_6$ clusters ($d_{yz}$ orbitals). Contour descriptions as in Fig. 3.

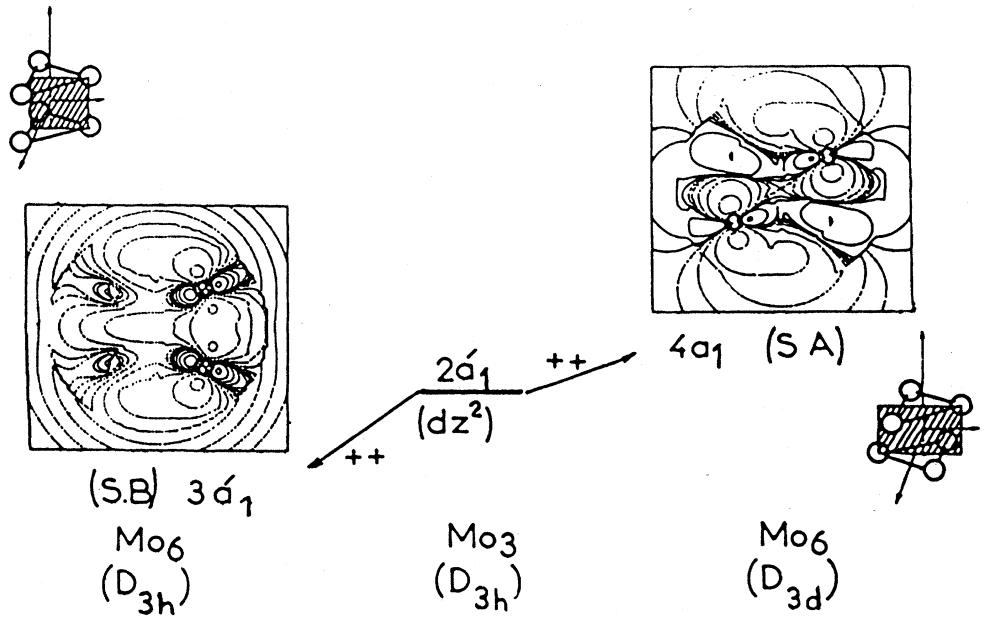


FIG. 6. Interactions of $d_z^2$ orbitals for the $D_{3h}$ and $D_{3d}$ stacking mode in $Mo_6$ clusters (see text for comments). Contour description as in Fig. 3.

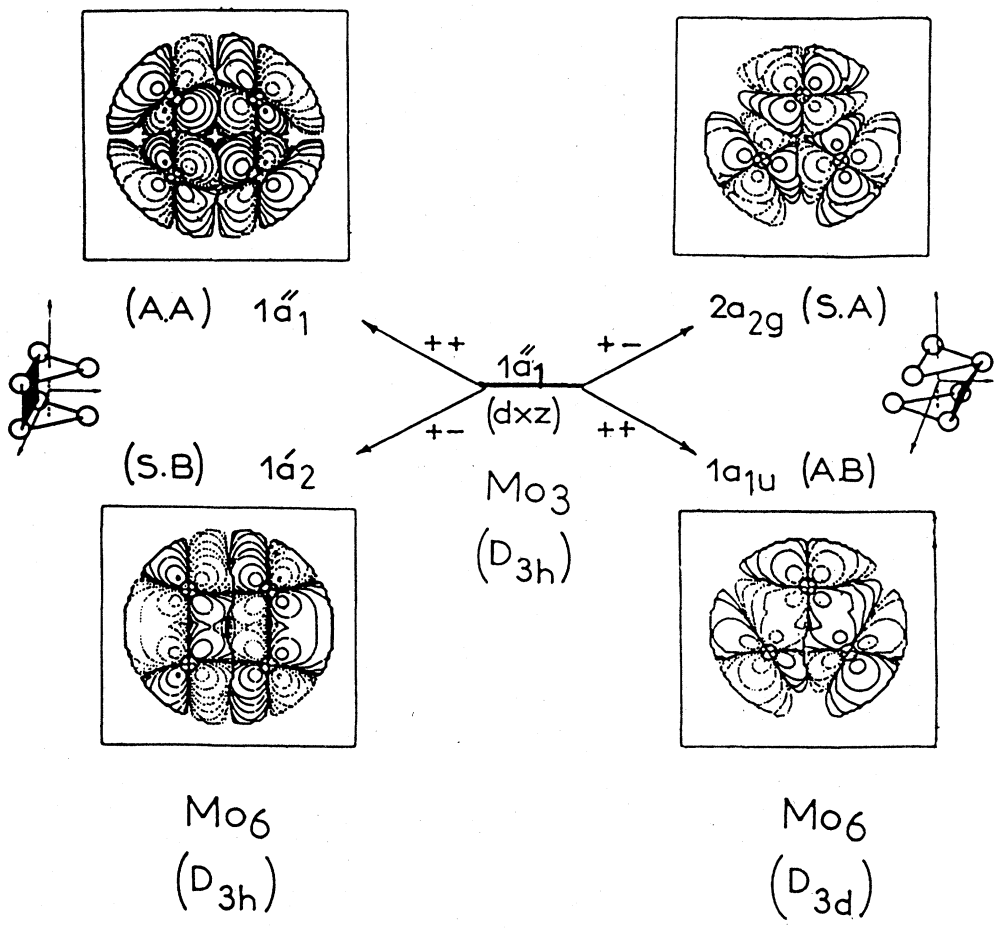


FIG. 7. Interactions of $d_{xz}$ orbitals for the $D_{3h}$ and $D_{3d}$ stacking mode in $Mo_6$ clusters (see text for comments). Contour description as in Fig. 3.

the increase of the number of metal-metal bonds: there are only 9 bonds in $D_{3h}$ while there are 12 in $D_{3d}$ clusters.

Obviously, this quantitative discussion rests very heavily upon "all other things being equal." Indeed, we shall take care to point out the inherent limitations of this fixed-geometry approach. A complete study of the energy surface, with metal-metal bond length and interlayer separation allowed to vary during the motion from $D_{3d}$ to $D_{3h}$, is beyond the scope of this paper.

Finally, the stabilization of an $O_h$ cluster with respect to the $D_{3d}$ one is illustrated by the orbital correlation diagram on the right-hand side of Fig. 4. This is the obvious consequence of the clearer separation between metal-metal bonding and antibonding levels [i.e., frontier orbitals $Mo_6(D_{3d})$ $1a_{1u}$-$3a_{2u}$; $Mo_6(O_h)$ $1t_{2u}$-$2t_{1u}$], which may be related to the perfect homogenization of the intra- and interplanar interactions. Indeed, the 12 metal-metal bonds directed along the edges of a $Mo_6$ octahedron form

TABLE I. Bonding energies.

| Unit | Average number of nearest neighbors per atom | Binding energy[a] per Mo atom (Ry) | Bond energy[b] (Ry) | Binding energy[c] per $Mo_3$ layer (Ry) |
|---|---|---|---|---|
| $Mo_3D_{3h}$ | 2 | 0.345 | 0.345 | |
| $Mo_6D_{3h}$ | 3 | 0.447 | 0.318 | 0.307 |
| $Mo_6D_{3d}$ | 4 | 0.480 | 0.240 | 0.400 |

[a]Based on the energy of an isolated Mo atom $4d^5 5s^1$, −7951.03 Ry.
[b]Obtained by dividing energy per Mo atom by the average number of bonds per Mo atoms (one-half of the number of nearest neighbors) (H. Basch *et al.*, Ref. 2).
[c]Based on the energy of an isolated $Mo_3D_{3h}$ unit, −23 854.125 Ry.

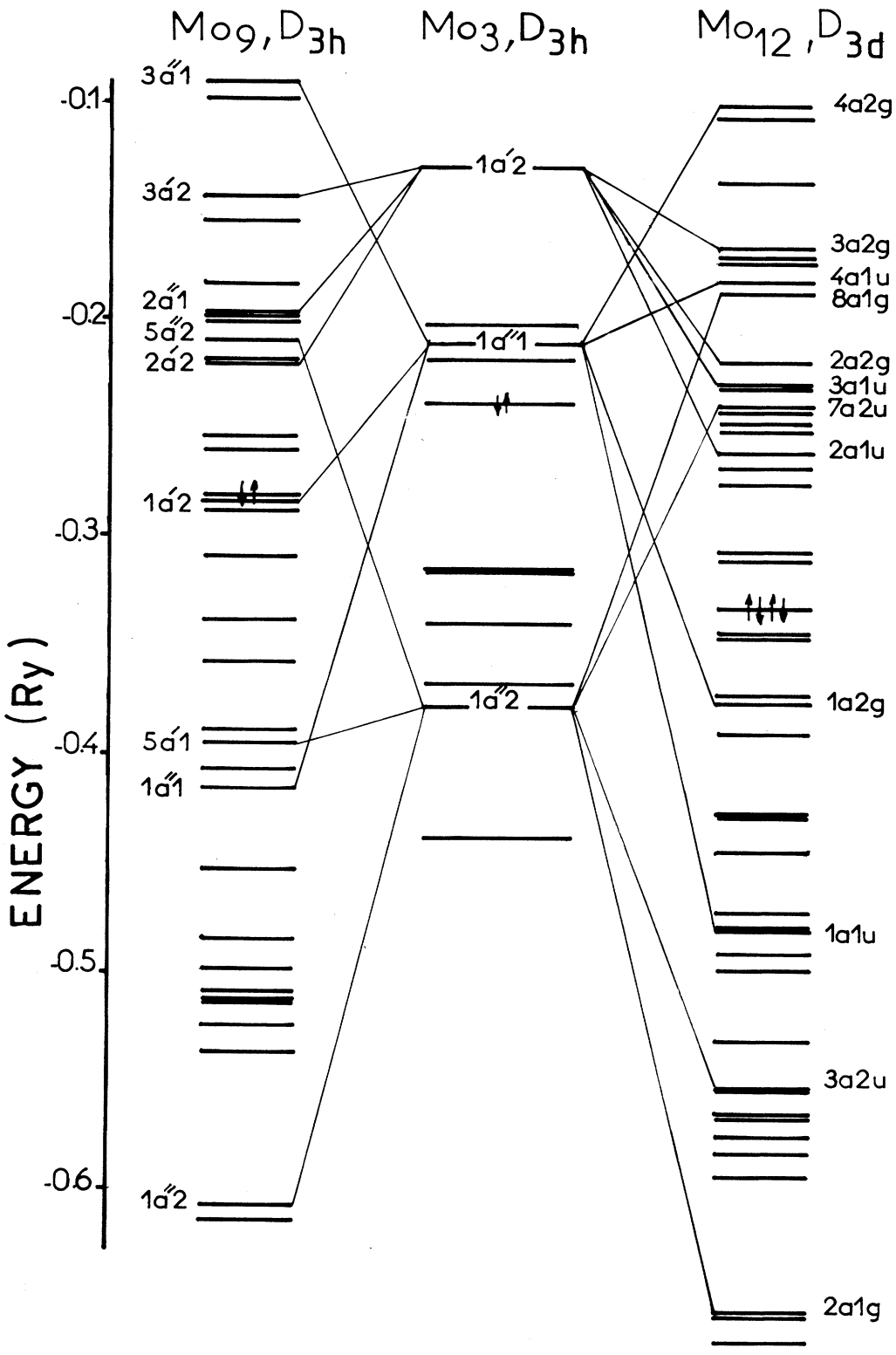


FIG. 8. Ground-state energy levels for $Mo_9$ and $Mo_{12}$ clusters. Arrows indicate the population of the highest-filled level.

a basis which can undergo transformations according to the $a_{1g}$, $t_{1u}$, $t_{2g}$, $e_g$, and $t_{2u}$ irreducible representations.[18]

### C. From $Mo_9(D_{3h})$ and $Mo_{12}(D_{3d})$ cluster to the extended metal-metal structure $(Mo_3)^1_\infty$

Turning to the $Mo_9$ and $Mo_{12}$ clusters, we will consider them as staggered groups, along the threefold axis, of three and four triangular metal layers, respectively. They are the successive terms of a series which has the extended linear-chain $(Mo_3)^1_\infty$ as a limit. The energy diagram obtained for these clusters is depicted in Fig. 8. The 11 parent levels of $Mo_3$ give rise to 33 ($Mo_9$) and 44 ($Mo_{12}$) levels, and the complexity in understanding the overall sets of MO's increases accordingly. We will therefore concentrate the discussion on the primary features only.

Viewing the staggered configuration of the layers, their mutual interactions are closely related to those of $Mo_6(D_{3d})$. However, the enhanced interactions arising from $\pi$-$Mo_3$ parent orbitals is evidenced by the increased splitting between bonding and antibonding paired orbitals. Indeed, the two interaction sets (i.e., $d_{xz}$ and $d_{yz}$) which play a crucial role in the construction of the cluster are now merged together. We have depicted in Fig. 9 contour maps of the $Mo_9$ wave functions involving $d_{xz}$ orbitals; they clearly exhibit identical although more extensive interactions than seen above for $Mo_6(D_{3d})$.

We will therefore turn our attention to the convergence behavior in the electronic patterns as the layer condensation proceeds. Thus the valence band width is not linear with the number of $Mo_3$ subunits. Rather it tends to a limit not yet reached for $Mo_{12}$. This is exemplified by the energy difference between the bonding and antibonding counterpart levels arising from the parent $1a_1''$ $Mo_3$ MO (e.g., $Mo_{12}$, 0.5779 Ry; $Mo_9$, 0.3255 Ry; $Mo_6$, 0.2396 Ry).

The second prominent point concerning these clusters is the advent of an "edge effect" due to the fact that the external layers do not undergo the same overall interactions as the internal layers do. This finds expression in some molecular orbitals which are then mainly localized on the external layers (e.g., $1a_2'$-$Mo_9$, $1a_{2g}$-$Mo_{12}$), the energy of which collapses with that of the frontier orbitals. In that way these orbitals may be compared to "surface states" of the solid in the forbidden energy band. In addition to the parity rule (i.e., odd or even number of layers) this edge effect must be related to the total number of layers (i.e., the larger the number, the weaker the edge effect).

In the extended linear chain, the edge effect vanishes, all the layers undergoing equivalent interactions. We now examine how the energy bands of the chain arise from the MO's of the individual clusters.[19]

To simplify the problem, let us imagine each $Mo_3$ layer as a hypothetical "pseudo atomic" unit with its appropriate system of $\sigma$ and $\pi$ orbital $x_i$. In order to go from finite clusters of atoms to the infinite solid we apply the Messmer model[20] which gives the solution of the eigenvalue and eigenvector problems of a simple tight-binding model for clusters of arbitrary size.

For a linear chain of $N$ atoms the expression of MO energy is given by

$$E_m = \frac{2t\cos[m\pi/(N+1)]}{1+2S\cos[m\pi/(N+1)]}, \quad m=1,2,\ldots,N \tag{1}$$

where $t$ is the transfer integral between nearest-neighbor atoms in the chain and $S$ is the nearest-neighbor overlap integral. Neglecting this overlap integral, as is usually the case in the tight-binding approximation, the eigenvalues are then given by

$$E_m = 2t\cos[m\pi/(N+1)], \quad m=1,2,\ldots,N \tag{2}$$

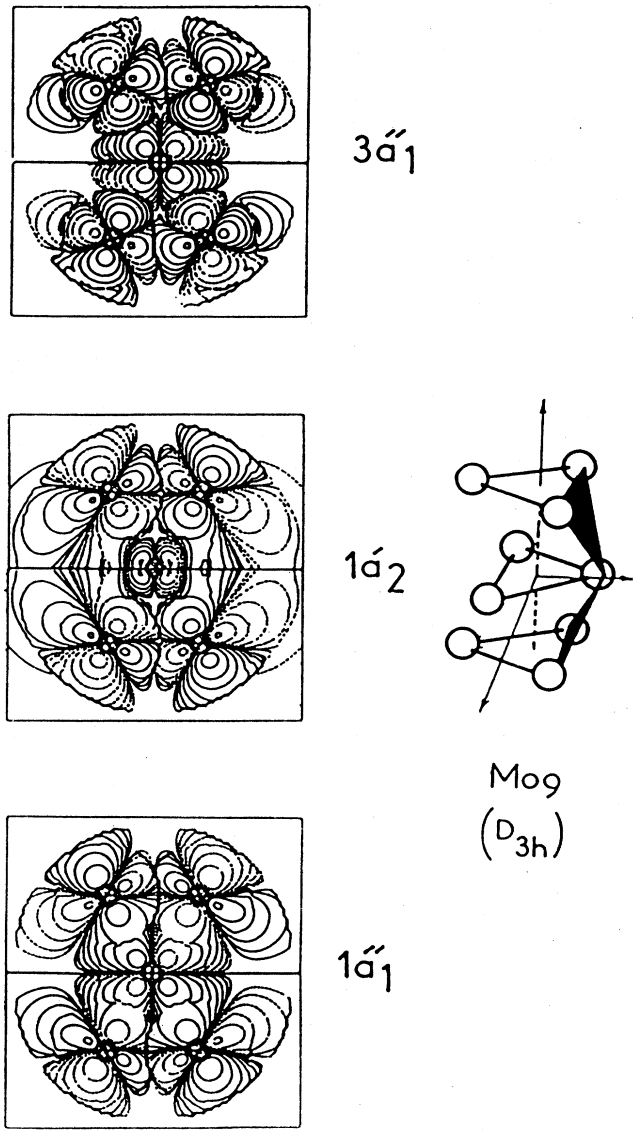


FIG. 9. $Mo_9$ wave-function contours of energy levels arising mainly from the interactions of $d_{xz}$ atomic orbitals. Contour description as in Fig. 3.

and the MO coefficients on the $\chi_i$ basis are

$$C_m^i = \left[\frac{2}{N+1}\right]^{1/2} \sin[im\pi/(N+1)], \quad i,m = 1,2,\ldots,N \ . \tag{3}$$

This result is analogous to that first derived by Coulson[21] for the conjugated polyenes.

In the upper part of Fig. 10 we have pictured the energy diagram obtained by Eq. (2). The scheme clearly shows, as $N$ increases up to infinity, the advent of an "energy band" physically terminated by the lower bonding MO $E_1$ (in-phase combination of the parent orbital) and by the upper antibonding MO $E_N$ (out-of-phase combination of the parent orbital). In this "$k$-independent" model the energy-band dispersion for an infinite chain is given by

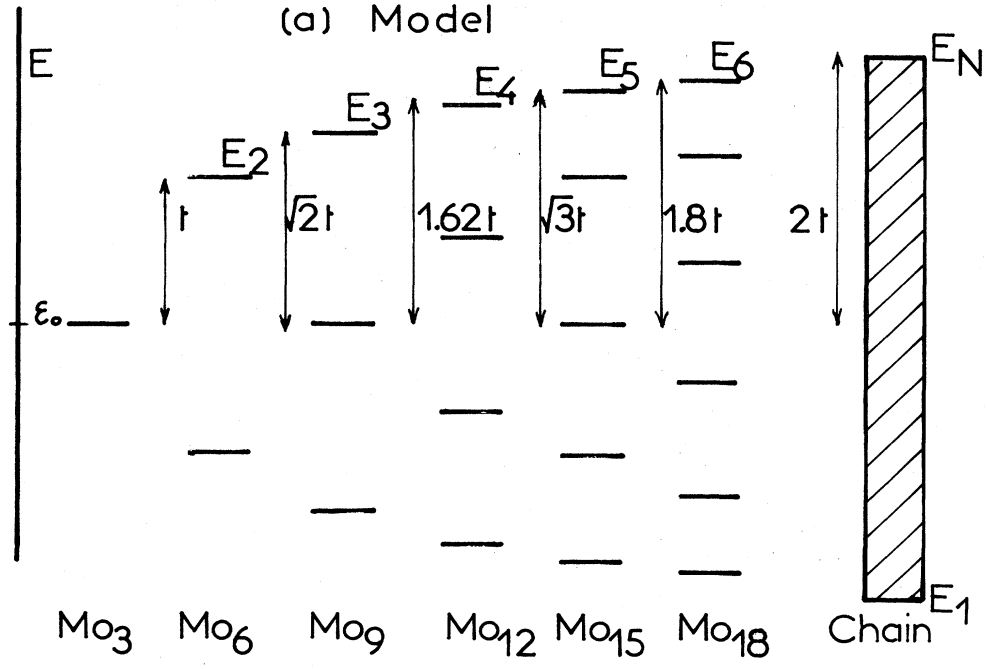


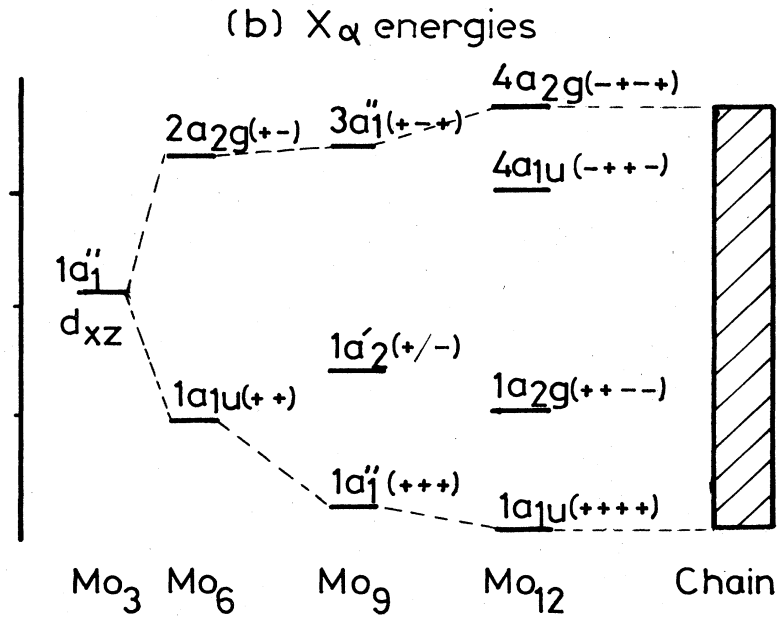


FIG. 10. Pattern for the widening of a parent molecular orbital of $Mo_3$ to an energy band represented as block diagrams (see text for comments).

$$E = E_N - E_1 = 4t \quad (4)$$

which corresponds to the energy dispersion of the "$k$-dependent" model,[22]

$$E(k) = \epsilon_0 - 2t\cos(ka), \quad 0 < k < \pi/a \quad (5)$$

with $a$ equal to interlayer separation.

In the lower part of Fig. 10 is depicted, for comparison purposes, the $X\alpha$ energy dispersion for levels originating from the $1a_1''$ ($d_{xz}$) $Mo_3$ MO. The analogy is evident; moreover, if we take for $t$ the half-splitting of $Mo_6$, we obtain for the model $2t = 0.1694$ Ry ($Mo_9$) and $1.618\ t = 0.1930$ Ry ($Mo_{12}$). Those values are close to the $X\alpha$ results 0.1675 Ry ($Mo_9$) and 0.1890 Ry ($Mo_{12}$). The small shift of the internal levels has to be attributed to the fact that the model is based on no mixing with another type of orbital, unlike $X\alpha$ calculations which exhibit a $\sigma$-$\pi$ mixing.

In Fig. 11 is gathered most of the information providing insight within the electronic structure of the pseudolinear chain: for sake of clarity the energy diagram is restricted to the part concerning the situation near the Fermi level. In the central part of the figure the discrete energy levels of finite clusters are pictured while, on each side, the corresponding energy-band schemes, seen as gathered block diagrams, are designed for the infinite chain. We shall discuss in detail only the band formation arising from the one-electron $1a_1''(d_{xz})$ and $1a_2'(d_{xy})$ MO's of the $Mo_3$ fragment allowed to be mixed by symmetry. Along the chain, only the $C_{3v}$ symmetry is conserved and gives rise to one double ($e$) and two single ($a_1$,$a_2$) degenerate representations. This combination of $d_{xz}$ orbitals leads to an $a_2$ band (see Fig. 10), likewise, the $a_2'$ MO ($d_{xy}$) generates a second $a_2$-type band. According to the energy of their originating levels, it might be expected that these two bands should largely overlap. However, on account of the noncrossing rule[23] concerning bands of the same symmetry, an avoided crossing takes place. The early bands mix and redistribute their orbital character (i.e., switch of the $d_{xz}$ and $d_{xy}$ character, or vice versa, going up through the new block diagrams) in order to create two new bands.

To summarize, the Fermi level is crossed by a broad $a_2$-type band ($d_{xz}$ orbitals) plus a narrow $e$ band. This band pattern gives rise to a low-dimensional conducting character which occurs through the overlap of $d_{xz}$ orbitals winding along the threefold axis (see Fig. 9). It corresponds to a high density of states at the Fermi level. This, together with a half-filled broadband, leads us to suggest a structural instability. Indeed such a metallic conductor chain of equidistant atoms (i.e., here equidistant layers) is unstable against dimerization. This instability, namely the Peierls's distortion,[24] is particularly important because it often drives a metal-to-insulator transition at low temperature.

Figure 11 also allows a discussion of this pairing distortion. Consider now the $Mo_{12}$ unit as if it were built up by two juxtaposed $Mo_6(D_{3d})$ fragments interacting with one another. If we go from the left to the right of the central part of Fig. 11, we can see the discrete eigenvalues corresponding to various stages of the separation of the $Mo_6$ fragments. The variation of the metal-metal interactions between the two $Mo_6$ units is clearly illustrated. Indeed the paired energy levels become narrower when we go from the left to the right which means that when the two $Mo_6$ units split apart the $Mo_{12}$ units converge in such a manner that they resemble $Mo_6$'s [i.e., $1a_{1u} + 1a_{2g}(Mo_{12}) \rightarrow 1a_{1u}(Mo_6)$]. Meanwhile, as the $Mo_6$'s separate, the symmetry breaks down. This leads to a splitting of the early broad conducting $a_2$ band into two

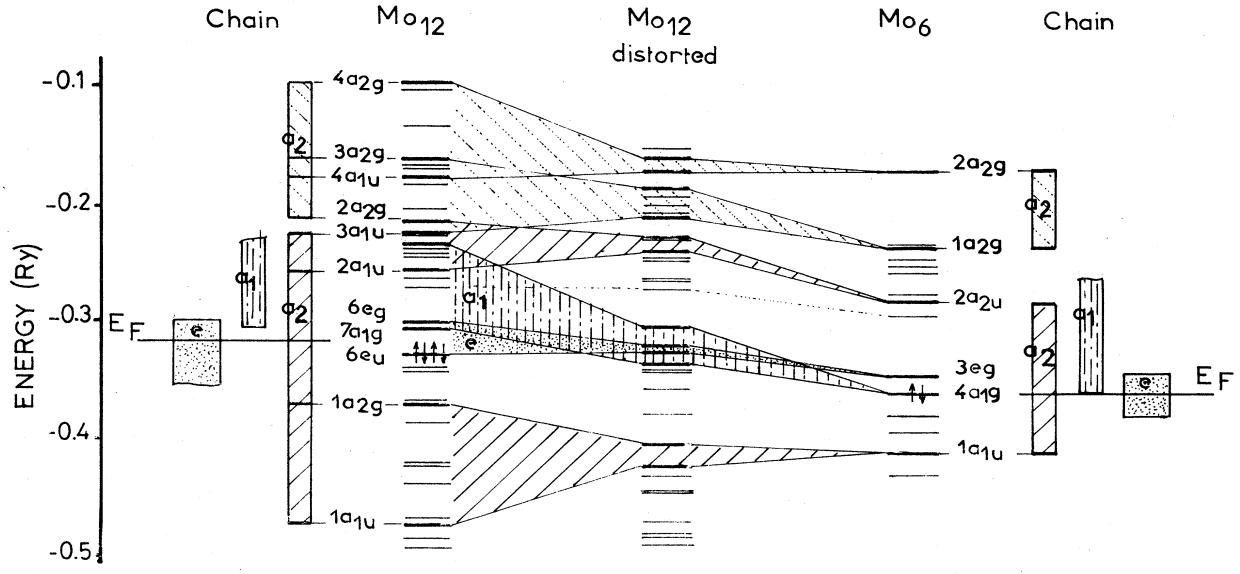


FIG. 11. Energy-band scheme arising from $Mo_6$ and $Mo_{12}$ molecular orbitals.

$a_2$ bands located on each side of the Fermi level. The contribution of these new bands to the conduction properties is then almost nonexistent. Furthermore, a lengthening of the Mo—Mo interunit distance of about 25% results in two very narrow bands ($a_1+e$) at the Fermi level with the advent of a real gap just above. It is obvious, then, that the quasi-one-dimensional conductor character has disappeared and we are reaching an insulator situation.

Finally, if we look at the discrete levels from right to left in Fig. 11, we get an alternative way to discuss the band structure of the chain. We have just to consider the chain, not as a stack of $Mo_3$ layers, but as a linear face-to-face condensation of $Mo_6$ subunits.

## IV. CONCLUSIONS

In this paper we investigated the intimate metal-metal interactions of bare metal aggregates. We gave an estimate of their strength and discuss their electronic structure. We have focused on the dominant interlayer interactions as the cluster dimension increases to the infinite chain and we have then shown the occurence of a broad conducting band winding around the stacking axis. Calculations are now in progress in order to extend this work, particularly to emphasize the interactions of such metallic systems with a ligand matrix of chalcogenide atoms.

## ACKNOWLEDGMENTS

We are grateful to Dr. I. Pruskil for helpful comments. The calculations were performed on the Bull DPS-8/70 M at the Centre Interuniversitaire de Calcul de Bretagne (CICB) of Rennes and on the Cray-1 at the Centre de Calcul Vectoriel pour la Recherche (CCVR)—Ecole Polytechnique-Palaiseau.

---

*Laboratoire associé au Centre National de la Recherche Scientifique no. 254.

[1]E. L. Mutterties, J. N. Rhodin, E. Band, C. F. Brucker, and W. R. Pretzer, Chem. Rev. **79**, 91 (1979); B. F. G. Johnson, *Transition Metal Clusters* (Wiley, New York, 1980); M. C. Manning and W. C. Trogler, Coord. Chem. Rev. **38**, 89 (1981); F. A. Cotton, *Reactivity of Metal-Metal Bonds,* Vol. 155 of the American Chemical Society, Symposium Series, edited by M. H. Chisholm (American Chemical Society, New York, 1981).

[2]R. P. Messmer, S. Knudson, K. H. Johnson, J. B. Diamond, and C. Y. Yang, Phys. Rev. B **13**, 1396 (1976); D. R. Salahub and R. P. Messmer, *ibid.* **16**, 2526 (1977); H. Basch, M. D. Newton, and J. B. Moskowitz, J. Chem. Phys. **73**, 4492 (1980); C. Bachmam, J. Demuynk, and A. Veillard, Faraday Symp. **14**, 71 (1980); E. C. Muetterties, Bull. Soc. Chim. Belg. **84**, 959 (1975); G. A. Ozin, Catal. Rev. Sci. Eng., **16**, 191 (1977); J. M. Basset and R. Ugo, in *Aspect of Homogenous Catalysis,* edited by R. Ugo (Reidel, Dordrecht, 1977), Vol. 3, p. 137; R. P. Messmer and D. R. Salahub, Phys. Rev. B **16**, 3415 (1977); K. Herman and P. S. Bagus, *ibid.* **17**, 4082 (1978); P. S. Bagus and M. Seel, *ibid.* **23**, 2065 (1980); R. P. Messmer, Surf. Sci. **106**, 225 (1981); D. R. Salahub and R. P. Messmer, *ibid.* **106**, 415 (1981); R. P. Messmer, D. R. Salahub, and S. H. Lamson, Phys. Rev. B **25**, 3576 (1982).

[3]A. Bino, F. A. Cotton, and Z. J. Dori, J. Am. Chem. Soc. **100**, 5252 (1978); **101**, 3842 (1979); **103** 243 (1981); A. Bino, F. A. Cotton, Z. J. Dori, and B. W. S. Kolthamner, *ibid.* **103**, 5779 (1981); M. Ardon, A. Bino, F. A. Cotton, Z. J. Dori, B. W. S. Kolthamner, and M. Karpon, Inorg. Chem. **20**, 4083 (1981); M. Ardon, A. Bino, F. A. Cotton, Z. J. Dori, M. Kaftory, and G. Reisner, *ibid.* **21**, 1912 (1982).

[4]R. Chevrel, M. Sergent, and J. Prigent, J. Solid State Chem. **3**, 515 (1971); M. Potel, R. Chevrel, and M. Sergent, Acta Crystallogr. Sect. B **76**, 1319 (1980); R. Chevrel, M. Potel, M. Sergent, M. Decroux, and O. Fischer, J. Solid State Chem **35**, 286 (1980); M. Potel, R. Chevrel, and M. Sergent, Acta Crystallogr. Sect. B **36**, 1545 (1980); M. Potel, Ph.D. thesis, University of Rennes, 1981; R. Chevrel and M. Sergent, in *Superconductivity in Ternary Compounds,* Vol. 32 of *Topics in Current Physics,* edited by O. Fischer and M. B. Maple (Springer, New York, 1981), Chap. 2.

[5]G. A. Ozin, Faraday Symp. Chem. Soc. **14**, 1 (1980); G. A. Ozin, M. P. Andrews, L. F. Nazar, H. X. Huber, and C. G. Francis, Coord. Chem. Rev. **48**(2), 203 (1983); R. C. Baetzold and J. F. Hamilton, Prog. Solid State Chem. **15**, 1 (1983).

[6]C. Y. Yang, K. H. Johnson, D. R. Salahub, J. Kaspar, and R. P. Messmer, Phys. Rev. B **24**, 5673 (1981).

[7]Similar structures have already been observed for Pt atoms [P. Longoni and P. Chini, J. Am. Chem. Soc. **98**, 7225 (1976)] and Ni atoms [C. A. Ghilardi, S. Midollini, and L. Sacconi, J. Chem. Soc. D **47** (1981)]. Nevertheless, the main interactions which cement the atoms in the cluster are those between metal atoms and the ligand atoms. Metal-metal interlayer interactions remain not significant.

[8]J. C. Slater, *Quantum Theory of Molecules and Solids* (McGraw-Hill, New York, 1974); K. H. Johnson, Adv. Quantum Chem. **7**, 143 (1973); H. Chermette, Folia Chim. Theor. Latina **IX**, 2 (1981).

[9]A. Le Beuze, M. A. Mackhyoun, R. Lissillour, and H. Chermette, J. Chem. Phys. **76**, 6060 (1982).

[10]K. Schwartz, Phys. Rev. B **6**, 2466 (1972).

[11]F. Herman and S. Skillman, *Atomic Structure Calculations* (Prentice-Hall, Englewood Cliffs, New Jersey, 1963).

[12]V. A. Gubanov, J. Weber, and J. W. D. Connolly, Chem. Phys. **11**, 319 (1975).

[13]H. Tatewaki, E. Miyoshi, and T. Nakamura, J. Chem. Phys. **76**, 5073 (1982); G. Del Conde, P. S. Bagus, and O. Novarro, Phys. Rev. B **25**, 7843 (1982); H. Basch, J. Am. Chem. Soc. **103**, 4657 (1982).

[14]M. C. Manning, D. E. Ellis, K. Berkowitz, and W. C. Trogler, Inorg. Chem. **21**, 2247 (1982); W. C. Trogler, D. E. Ellis, and J. Bakowitz, J. Am. Chem. Soc. **101**, 5896 (1979); B. E. Burstein, F. A. Cotton, J. C. Green, E. A. Seddon, and R. G. Stanley, *ibid.* **102**, 955 (1980). For a review on electronic structure of transition-metal cluster complexes, see M. C. Manning and W. C. Trogler, Coord. Chem. Rev. **38**, 89 (1981).

[15]B. E. Burstein, F. A. Cotton, N. B. Hall, and R. C. Najjar,

Inorg. Chem. **21**, 9P2 (1982).

[16]This picture has been proposed earlier for $\sigma$ orbitals. See B. E. R. Schilling and R. Hoffman, J. Am. Chem. Soc. **101**, 3456 (1979).

[17]W. L. Jorgensen and L. Salem, *The Organic Chemist's Book of Orbitals* (Academic, New York, 1973).

[18]S. F. A. Kettle, Theor. Chim. Acta (Berlin) **3**, 211 (1965).

[19]This truncated-crystal approach has already been used to obtain a quasi-band-like picture of energy states. See R. P. Messmer and G. D. Watkins, Phys. Rev. B **7**, 2568 (1973); A. Zunger, J. Phys. C **7**, 76 (1974); J. K. Burdet, in *Structures and Bonding in Crystal I,* edited by M. O. Keeffe and A. Navrotsky (Academic, New York, 1981), Chap. 11; E. P. Larkins, J. Phys. Chem. Solids **4**, 3065 (1971); D. R. Salahub and R. P. Messmer, Phys. Rev. B **14**, 2592 (1976). F. Herman, D. R. Salahub, and R. P. Messmer, *ibid.* **16**, 2433 (1977).

[20]R. P. Messmer, Phys. Rev. B **15**, 1311 (1977).

[21]C. A. Coulson, Proc. R. Soc. London Ser. A **169**, 413 (1939); W. E. Moffitt and C. A. Coulson, Trans. Faraday Soc. **44**, 81 (1948).

[22]J. R. Reitz, *Solid State Physics,* edited by H. Ehrenreich, F. Seitz, and D. Turnbull (Academic, New York, 1955), Vol. 1, p. 2.

[23]C. A. Coulson, *Valence,* 2nd ed. (Oxford University Press, London, 1969), p. 68.

[24]R. E. Peierls, *Quantum Theory of Solids* (Oxford University Press, London, 1955); L. Alcacer, *The Physics and Chemistry of Low Dimensional Solids* (Reidel, Dordrecht, 1980).